Research Journal of Pharmacognosy (RJP) 8(4), 2021: 37–51
Received: 29 May 2021
Accepted: 10 Aug 2021
Published online: 22 Aug 2021
DOI: 10.22127/RJP.2021.288366.1705

Original article

In Silico Study of Some Natural Anthraquinones on Matrix Metalloproteinase Inhibition

Amir Taherkhani[1], Shirin Moradkhani[2], Athena Orangi[3], Alireza Jalalvand[4], Zahra Khamverdi[3*]

[1]Research Center for Molecular Medicine, Hamadan University of Medical Sciences, Hamadan, Iran.
[2]Department of Pharmacognosy, School of Pharmacy, Medicinal Plants and Natural Product Research Center, Hamadan University of Medical Sciences, Hamadan, Iran.
[3]Dental Research Center, Department of Restorative Dentistry, Dental School, Hamadan University of Medical Sciences, Hamadan, Iran.
[4]Department of Influenza and Other Respiratory Viruses, Pasteur Institute of Iran, Tehran, Iran.

Abstract

Background and objectives: Matrix metalloproteinase-13 (MMP-13) is a proteolytic enzyme playing an important role in the activation of the MMP cascade, which seems to be vital in both bone metabolism and homeostasis. However, the up-regulation of MMP-13 is involved in developing several human disorders such as aggressive tumors, tooth decay, rheumatoid arthritis, osteoarthritis, skin ageing, and Alzheimer's disease. We performed a molecular docking analysis to discover the potential MMP-13 inhibitors in a total of 21 anthraquinone derivatives. **Methods:** The binding affinity of the tested compounds to the MMP-13 catalytic site was estimated by the Autodock 4.0 software. Moreover, the stability of the docked pose of the top-ranked compounds were examined using molecular dynamics simulations. **Results:** Pulmatin, sennidin A, emodin-8-glucoside, emodin, rhodoptilometrin, chrysophanol, knipholone, sennidin B, aloe emodin 8-glucoside, and aloe-emodin demonstrated considerable binding affinity to the MMP-13 active site. However, the molecular dynamics simulations showed that the docked poses of sennidin A and sennidin B were not considerably stable. **Conclusion:** The present study suggested that pulmatin, emodin-8-glucoside, emodin, rhodoptilometrin, chrysophanol, knipholone, aloe emodin 8-glucoside, and aloe-emodin may be considered as drug candidates for therapeutic applications in many human diseases. However, the validation of this finding is needed in the future.

Keywords: anthraquinones; cancer; matrix metalloproteinase-13; MMP inhibitor; molecular docking

Citation: Taherkhani A, Moradkhani Sh, Orangi A, Jalalvand A, Khamverdi Z. In silico study of some natural anthraquinones on matrix metalloproteinase inhibition. Res J Pharmacogn. 2021; 8(4): 37–51.

Introduction

Matrix metalloproteinases (MMPs) are zinc and calcium-containing enzymes taking part in degrading the extracellular matrix. Accordingly, MMP-13 (collagenase-3), which belongs to the MMP major family, is involved in many normal biological procedures within the human cells, including bone-building, tissue remodeling, and wound healing [1, 2]. The overexpression and/or hyperactivity of MMP-13 have been found to be associated with developing several human diseases such as rheumatoid arthritis and osteoarthritis [3-5]. A positive correlation has been observed in previous studies between the elevated expression of MMP-13 and the initiation/progression of both aggressive tumors and metastasis. Additionally, it has been demonstrated that collagenase-3 is up-regulated in several malignant tumors, including breast cancer, head and neck cancers, chondrosarcomas, and basal cell carcinomas in the skin [6,7]. Also,

*Corresponding author: z_khamverdi@umsha.ac.ir

previous studies have reported that MMPs take a part in the tooth caries' progression [8-11]. In a study, Vasconcelos et al. [12] demonstrated that the single nucleotide polymorphism rs478927 in MMP-13 is correlated with caries' occurrence as well as developmental defects of enamel in children. Moreover, MMP-13 was shown to contribute to skin ageing [13]. Therefore, MMP-13 inhibition may be useful in the treatment of the above-mentioned disorders and also in developing new effective MMP inhibitors with low toxicity, which will be of interest to scientists in the future studies [13]. It may be suggested that MMP-13 inhibition could possibly lead to the prevention and/or therapeutic procedures of several human disorders such as cancer, osteoarthritis, rheumatoid arthritis, skin ageing, and dental caries.

Molecular docking analysis is widely used to predict the potential inhibitors for certain proteins/enzymes involved in human disorders. It is known as a rapid and inexpensive approach used to estimate the binding affinity of drug candidates to the active site of target proteins [2, 14-21]. Plant-based compounds, due to their lower toxicity and higher availability, have always been of interest to scientists for drug discovery [22].

Anthraquinones (AQs), that naturally occur in plants, are secondary metabolites mostly found in the families of Polygonaceae, Rubiaceae, and Rhamnaceae, as well as in fungi and lichens. AQs have been considered as natural food coloring substances and have shown several therapeutic effects in human disorders. They are made up of 9,10-anthracenedione to which different chemical groups are attached (e.g., hydroxyl, methyl, carboxyl, etc.) [23,24]. Figure 1 demonstrates the backbone of AQ derivatives achieved by the ACD/ChemSketch version 12.01. Several AQs have been previously revealed to have therapeutic effects in various human disorders, including cancer [25,26], osteoarthritis [27], rheumatism [28], memory loss, inflammation, skin-ageing [29,30], and dental caries [2]; however, their mechanism of action has not been clearly understood yet [27]. While Ha et al. [31] in their study demonstrated that emodin could lead to the decreased expressions of MMP-1 and MMP-13 at the mRNA level. Besides, Emodin and obtusifolin were found to contribute to the downregulation of the MMP-3 and MMP-13 at both the mRNA and protein levels [27,32].

In the present study, we hypothesized that AQs, by binding to the catalytic domain of MMP-13, may act as the inhibitors of the enzyme. Therefore, to examine our hypothesis, we designed a molecular docking study for examining the binding affinity of several known AQs to the MMP-13 catalytic site (Supplementary Table). Additionally, molecular dynamics (MD) simulations were conducted to investigate the stability of docked pose of the top ranked AQs, in order to achieve more reliable results.

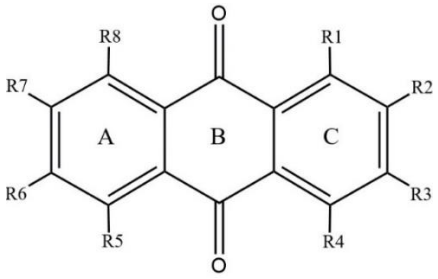

Figure 1. Basic structure of anthraquinones; R: -OH, -CH3, -OCH3, -CH2OH, -CHO, -COOH

Materials and Methods

Ethical considerations

We considered ethics in research in our study. The present study was approved by the Ethics Committee of Hamadan University of Medical Sciences, Hamadan, Iran (ethics no. IR.UMSHA.REC.1398.576).

Structural preparing, molecular docking, and dynamics simulations

The three-dimensional structures of MMP-13 along with AQ derivatives, which were considered as ligands in the current study, were achieved from the Research Collaboratory for Structural Bioinformatics (RCSB) and the PubChem databases available at https://www.rcsb.org [33] and https://pubchem.ncbi.nlm.nih.gov [34], respectively. The 5B5O file included the three-dimensional coordinates of MMP-13 as well as the inhibitor of the enzyme (PDB ID: WMM) in the Nara et al.'s [35] study at 1.2 Å x-ray resolution. The molecular energy of MMP-13 and small molecules were minimized before the estimation of the binding affinity between the MMP-13 catalytic site and AQ derivatives. Swiss-pdbViewer version 4.1.0

(http://www.expasy.org/spdbv) and HyperChem version 8.0.10 were used for the MMP-13 and small molecules' energy minimization, respectively [36,37]. The molecular docking analysis was then completed by the AutoDock software (version 4.0), which is available at http://autodock.scripps.edu [38]. The Lamarckian Genetic Algorithm was used by AutoDock to estimate the affinity of binding ($\Delta G_{binding}$) between the receptor and ligand. More details about the method used in this study such as its grid box settings and the amino acids recognized as the docking pocket, have been reported in our previous report [2].

We performed the molecular dynamics simulations to examine the stability of docked poses of the top-ranked AQs (top-10 AQs with the *K*i value at the nanomolar scale) within the MMP-13 active site. Correspondingly, this was performed using the Discovery Studio Client version 16.1.0.15350 with the following settings: molecular dynamics simulation time, 1-nanosecond (1ns); temperature, 310 K; solvent, water; and force field, CHARMm.

Oral bioavailability study

The drug-likeness of the AQ derivatives were predicted in terms of the Rule of Five (RO5), which has been well-presented in a study by Lipinski et al. [39]. The chemo-physical properties of the ligands were investigated using the PubChem database. According to the RO5, drug candidates to be considered suitable for oral use, can only violate one of the following four rules: molecular mass $\leq$ 500 gr/mol, log of the partition coefficient between octanol and water (LogP) $\leq$ 5, number of accepting hydrogen bonds $\leq$ 10, and number of hydrogen bond donors $\leq$ 5.

Results and Discussion

According to the results of the docking analysis, it was demonstrated that, in total, 10 AQ derivatives, including pulmatin (chrysophanol-8-0-glucoside), sennidin A (SA), emodin-8-glucoside, emodin, rhodoptilometrin, chrysophanol, knipholone, SB, aloe emodin 8-glucoside, and aloe-emodin can potentially bind to the MMP-13 catalytic site at the nanomolar concentration. The $\Delta G_{binding}$ for these compounds were estimated to range from -9.76 kcal/mol (for pulmatin) to -8.23 kcal/mol (for aloe-emodin) (Figure 2). In our previous study, to compare the binding affinity of top-ranked flavonoids with the MMP-13 standard inhibitors, a total of five MMP-13 control inhibitors, including BP4 (PDB ID: 5289110), MMP9/MMP13 inhibitor (PDB ID: 9983251), actinonin (PDB ID: 443600), PD166793 (PDB ID: 9918908), and WMM (PDB ID: 2366268) were docked with the MMP-13 catalytic site [2]. Among the control inhibitors, the best binding affinity was calculated for BP4 with the $\Delta G_{binding}$ of -8.63 kcal/mol. According to the results of the present study, the binding affinity of the top-six MMP-13 inhibitors to the MMP-13 active site was found to be higher than that of BP4. The $\Delta G_{binding}$ and inhibition constant (*K*i) value of all the AQ derivatives tested in this study are listed in Table 1. Moreover, the details of energies achieved from docking analysis of the top-10 compounds are illustrated Table 2. All interactions between ligand and residues within the MMP-13 active site were identified for the top-10 AQs using the BIOVIA Discovery Studio Visualizer 19.1.0.18287 available at https://discover.3ds.com/discovery-studio-visualizer-download. These interactions were compared once before and once after the molecular dynamics simulations and are presented in Table 3 and Figure 3. All hydrogen bonds with a distance longer than 5 Å were considered as insignificant. Figure 4 illustrates the interactions between the top-10 AQs in this study as well as the residues within the MM-13 catalytic domain in a single network. Accordingly, this was constructed using the Cytoscape software, which is available at https://cytoscape.org/download.html [40].

In this study, the top-10 MMP-13 inhibitors were considered for drug-likeness analysis, based on the RO5 described in a study by Lipinski et al. [39]. According to the obtained results, eight of the AQ derivatives, including pulmatin (chrysophanol-8-0-glucoside), emodin-8-glucoside, emodin, rhodoptilometrin, chrysophanol, knipholone, aloe emodin 8-glucoside, and aloe-emodin due to their number of violations from RO5, were considered as orally active drugs (Table 4).

Previous studies performed in this field have linked the up-regulation of MMP-13 to the pathogenesis of several human disorders, including aggressive tumors, tooth caries, rheumatoid, osteoarthritis, and Alzheimer's disease [3-11, 41, 42] Besides, AQs are bioactive agents widely considered as potential anticancer compounds.

Table 1. Estimated energy of binding and inhibition constant values of 21 anthraquinone derivatives with matrix metalloproteinase-13 achieved from molecular docking analysis

PubChem ID	Ligand name	Estimated energy of binding (kcal/mol)	*Ki*
442731	Pulmatin (Chrysophanol 8-O-glucoside)	-9.76	70.58 nM
92826	Sennidin A	-9.65	84.50 nM
99649	Emodin-8-glucoside	-9.07	224.35 nM
3220	Emodin	-8.94	279.97 nM
101286218	Rhodoptilometrin	-8.93	285.97 nM
10208	Chrysophanol	-8.83	338.39 nM
442753	Knipholone	-8.55	541.41 nM
10459879	Sennidin B	-8.51	574.78 nM
126456371	Aloe Emodin 8-Glucoside	-8.49	594.84 nM
10207	Aloe-emodin	-8.23	929.88 nM
3083575	Obtusifolin	-8.10	1.15 uM
361510	Emodic acid	-8.07	1.22 uM
10168	Rhein	-7.98	1.41 uM
2950	Danthron	-7.96	1.47 uM
3663	Hypericin	-7.77	2.02 uM
6683	Purpurin	-7.77	2.03 uM
10639	Physcion	-7.69	2.29 uM
6293	Alizarin	-7.57	2.81 uM
2948	Damnacanthal	-7.31	4.35 uM
124062	Rubiadin	-7.11	6.13 uM
160712	Nordamnacanthal	-6.57	15.25 uM

Ki, inhibition constant

Table 2. Details of energies between top-10 anthraquinone derivatives and matrix metalloproteinase-13 active site calculated from docking study

Ligand name	Final intermolecular energy(kcal/mol)	Final total internal energy (kcal/mol)	Torsional free energy (kcal/mol)	Unbound systems energy (kcal/mol)	Estimated free energy of bindind (kcal/mol)
Pulmatin (Chrysophanol 8-O-glucoside)	-9.91	-3.22	2.39	-0.99	-9.76
Sennidin A	-6.92	-7.14	2.68	-1.73	-9.65
Emodin-8-glucoside	-9.14	-3.61	2.68	-0.99	-9.07
Emodin	-9.24	-1.1	0.89	-0.5	-8.94
Rhodoptilometrin	-9.53	-1.28	1.79	-0.09	-8.93
Chrysophanol	-8.84	-1.11	0.6	-0.53	-8.83
Knipholone	-9.39	-2.53	2.09	-1.28	-8.55
Sennidin B	-8.2	-5.23	2.68	-2.24	-8.51
Aloe Emodin 8-Glucoside	-7.58	-4.87	2.98	-0.98	-8.49
Aloe-emodin	-9.39	-1.12	1.19	-1.09	-8.23

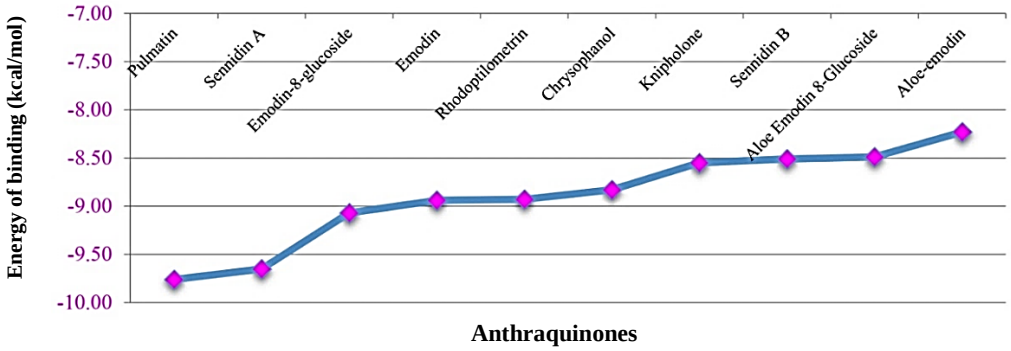

Figure 2. The estimated binding energy of top-10 MMP-13 inhibitors with considerable inhibition constant values at the nanomolar scale; MMP-13: matrix metalloproteinase-13

Table 3. Interactions formed between top-10 anthraquinone derivatives and amino acids inside the matrix metalloproteinase-13 catalytic site, before and after MD simulations

Ligand name	Hydrogen bond (distance Å)	Hydrophobic interaction (distance Å)	Miscellaneous (distance Å)
Pulmatin (before MD)	Gly183 (4.57 [classical]); Tyr244 (4.95 [classical]); Glu223 (4.00* [classical]); Ala186 (4.02 [classical])	Gly183 (4.37 [pi-pi], 4.95 [pi-pi]); Leu184 (5.36 [pi/alkyl]); Ile243 (5.78 [pi/alkyl])	NA
Pulmatin (after MD)	Glu223 (4.69 [classical]); Ala186 (4.94 [non-classical])	NA	NA
Sennidin A (before MD)	NA	His232 (7.92 [pi-pi]); Leu184 (5.43 [pi-alkyl]); Pro242 (6.75 [pi-alkyl])	NA
Sennidin A (after MD)	NA	NA	NA
Emodin-8-glucoside (before MD)	NA	Leu184 (5.63 [pi-alkyl])	NA
Emodin-8-glucoside (after MD)	Pro242 (4.33 [classical], 4.79 [non-classical], 4.06 [non-classical]); Lys234 (3.86 [non-classical])	NA	NA
Emodin (before MD)	Ala186 (2.64 [classical]); Ile243 (4.70 [non-classical])	His232 (5.80 [pi-alkyl], 6.21 [classical]); Pro242 (4.65 [pi-alkyl], 4.79 [alkyl]); Leu185 (5.35 [pi-alkyl])	Pro242 (4.65 [Lone Pairs])
Emodin (after MD)	Tyr244 (4.88 [classical]); Gly183 (2.99 [classical])	NA	NA
Rhodoptilometrin (before MD)	Ala186 (2.34 [classical]); Ile243 (4.51 [non-classical])	His222 (5.45 [pi-alkyl]); Leu185 (4.48 [alkyl]); Val219 (4.66* [alkyl]); Pro242 (4.13 [pi-alkyl], 5.23 [pi-alkyl])	NA
Rhodoptilometrin (after MD)	Glu223 (4.81 [classical])	His222 (4.80 [pi-pi], 4.80 [pi-pi], 6.17 [pi-pi]); Val219 (4.35 [alkyl]); Leu218 (4.65 [alkyl]); Met240 (4.54 [alkyl])	NA
Chrysophanol (before MD)	Ile243 (4.64 [non-classical])	His232 (5.81 [pi-alkyl], 6.22 [pi-pi]); Pro242 (4.66 [pi-alkyl], 4.69 [alkyl]); Leu185 (5.33 [pi-alkyl])	Pro242 (4.66 [Lone Pairs])
Chrysophanol (after MD)	Leu223 (4.19 [classical]); Pro242 (4.07 [classical], 4.60 [non-classical])	His222 (4.48 [pi-pi], 5.38 [pi-pi], 5.38 [pi-pi]); Val219 (6.50 [pi-alkyl])	NA
Knipholone (before MD)	Gly183 (3.14 [classical]); Ile243 (3.96 [non-classical])	Pro242 (5.09* [pi-alkyl]); Ile243 (4.97 [pi-alkyl], 5.04 [alkyl])	Pro242 (5.23 [Lone Pairs])
Knipholone (after MD)	Ala186 (3.27 [classical]); Glu223 (4.88 [classical]); Pro242 (3.97 [classical])	Leu184 (5.31 [pi-pi]); Phe241 (6.44 [pi-pi]); Phe241 (6.18 [pi-alkyl]); Leu184 (4.64 [pi-alkyl], 4.64 [pi-alkyl]); Pro242 (4.15 [pi-alkyl], 4.48 [pi-alkyl], 4.48 [pi-alkyl]); Leu185 (5.24 [pi-alkyl])	NA
Sennidin B (before MD)	NA	Gly183 (4.74 [pi-alkyl]); Pro242 (5.95 [pi-alkyl], 6.18 [pi-alkyl])	NA
Sennidin B (after MD)	Pro242 (3.80 [classical])	NA	NA
Aloe Emodin 8-Glucoside (before MD)	Ser182 (4.19 [classical])	NA	NA
Aloe Emodin 8-Glucoside (after MD)	Leu184 (4.68 [classical]); Ser182 (3.97 [non-classical]); Gly183 (3.69 [non-classical], 3.94 [non-classical]); Pro242 (4.91 [non-classical])	NA	NA
Aloe-emodin (before MD)	Ile243 (4.63 [non-classical])	His232 (6.20 [pi-pi]); Pro242 (4.65* [pi-alkyl]); Leu185 (5.34 [pi-alkyl])	Pro242 (4.65 [Lone Pairs])
Aloe-emodin (after MD)	His222 (4.14 [classical]); Ser182 (3.93 [classical], 4.17 [classical], 3.93 [non-classical])	His222 (6.77 [pi-pi], 6.73 [pi-pi]); Val219 (6.99 [pi-alkyl]); Pro242 (4.49 [pi-alkyl], 4.59 [pi-alkyl])	NA

*:MD, molecular dynamics

Table 4. Chemo-physical properties of top-10 anthraquinone derivatives associated with the Lipinski's rule of five

Ligand name	Molecular weight (g/mol)	LogP	Hydrogen Bond Donor Count	Hydrogen bond acceptor count	Number of violations from RO5	Orally active drug
Pulmatin (Chrysophanol 8-O-glucoside)	416.4	1.3	5	9	0	Yes
Sennidin A	538.5	4.8	6	10	2	No
Emodin-8-glucoside	432.4	0.9	6	10	1	Yes
Emodin	270.24	2.7	3	5	0	Yes
Rhodoptilometrin	314.29	2.4	4	6	0	Yes
Chrysophanol	254.24	3.5	2	4	0	Yes
Knipholone	434.4	4.2	4	8	0	Yes
Sennidin B	538.5	4.8	6	10	2	No
Aloe Emodin 8-Glucoside	432.4	0	6	10	1	Yes
Aloe-emodin	270.24	1.8	3	5	0	Yes

LogP: the logarithm of the partition coefficient between n-octanol and water; RO5: rule of five

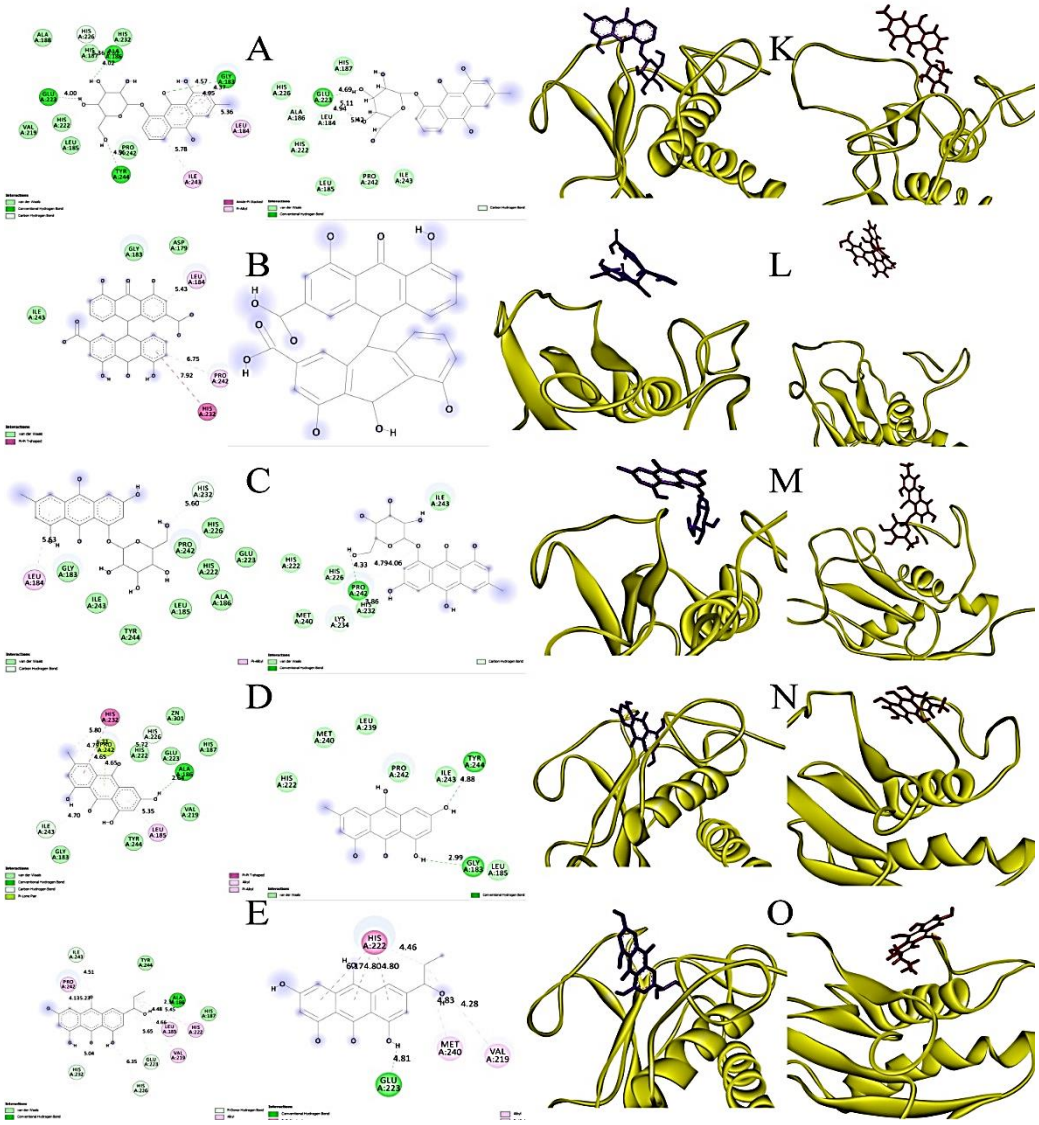

Figure 3. Images from (A) to (J) illustrate two-dimensional interactions, while images from (K) to (T) demonstrate three-dimensional docked pose, in which left and right images were achieved from docking and molecular dynamics simulations, respectively: (A and K): pulmatin; (B and L): sennidin A; (C and M): emodin-8-glucoside; (D and N): emodin; (E and O): rhodoptilometrin; (F and P): chrysophanol; (G and Q): knipholone; (H and R): sennidin B; (I and S): aloe emodin 8-glucoside; (J and T): aloe-emodin with the residues within the MMP-13 catalytic site

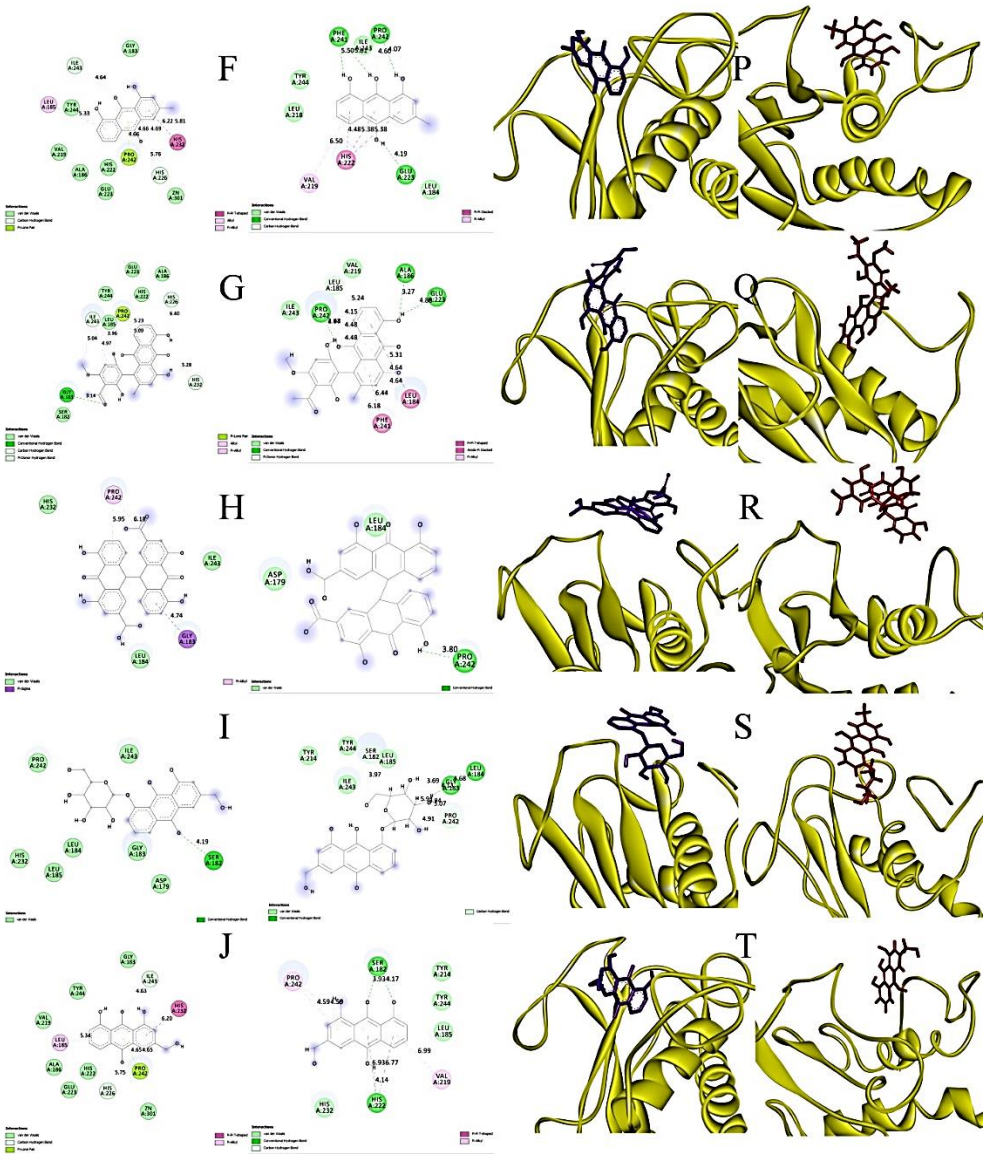

Figure 3. Continued

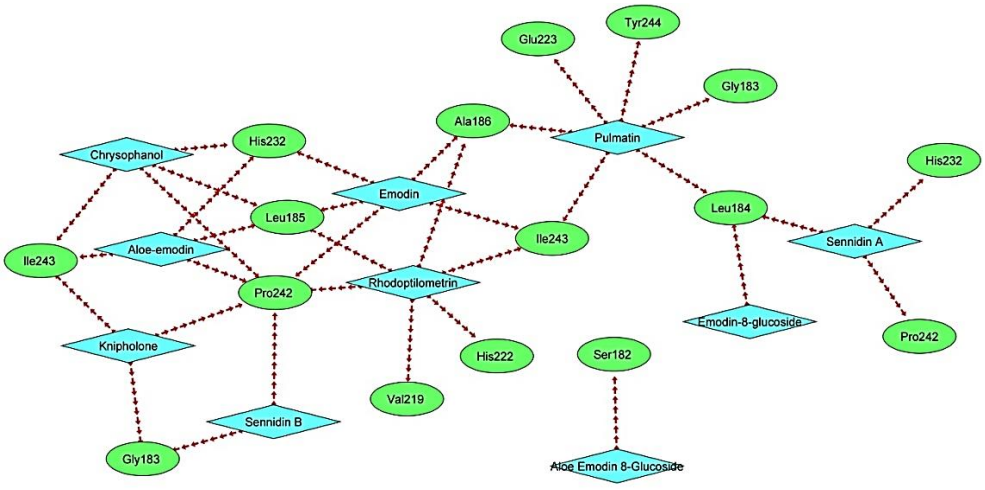

Figure 4. Interactions between top-10 compounds and the residues inside the MMP-13 catalytic site

Many other beneficial properties, including anti-tooth caries and anti-osteoarthritis activities, have been reported for AQs; however, their mechanism of action has not been clearly understood yet [27,43]. In a previous study by Uzun et al. [13], a molecular docking analysis was performed to evaluate the binding affinity of AQ, flavonoid, tannin, and naphthalene main skeletons to MMP-1, MMP-8, and MMP-13. As a result, the authors reported that the estimated binding energy between AQ main skeleton and MMP-13 was -7.6 kcal/mol, illustrating that AQs can potentially inhibit MMP-13. However, to the best of our knowledge, the present study is the first research in which a total of 21 AQ derivatives were investigated to identify the potential MMP-13 inhibitors using molecular docking analysis. Beside the study performed by Uzun *et al*. [13], the authors in the current study investigated the inhibitory effect of several AQ derivatives on MMP-13 at different concentrations. Furthermore, Uzun et al. [13] demonstrated that pulmatin, emodin-8-glucoside, emodin, chrysophanol, aloe-emodin, rhein, and phycion inhibited 65.17, 43.61, 42.37, 74.95, 59.07, 52.92, and 68.39% of the MMP-13 activity at the concentration of 100 µg/mL, respectively. The authors performed their study using the inhibitory activity screening assay kits.

According to the results of the present study, pulmatin was shown to have the best binding affinity to the MMP-13 catalytic site with a $\Delta G_{binding}$ of -9.76 kcal/mol followed by sennidin A, emodin-8-glucoside, emodin, rhodoptilometrin, chrysophanol, knipholone, sennidin B, aloe emodin 8-glucoside, and aloe-emodin, respectively. In addition, it was estimated that the top-10 compounds can considerably block the MMP-13 catalytic site at the nanomolar scale.

Pulmatin (chrysophanol-8-*0*-glucoside) is an AQ mostly identified within rhubarb, as a well-known rhizome of the *Rheum* genus such as *Rheum tanguticum*, *Rheum palmatum*, *Rheum officinale*, and *Rheum undulatum*, which are frequently used in traditional medicine [44-46]. Seo et al. [44] in their study reported that pulmatin had an inhibitory effect on collagen and thrombin induced-platelet aggregation in vivo. In another study, Siegers et al. [46] reported that chrysophanol 8-O-glucoside could considerably down-regulate the expressions of smooth muscle alpha-actin (α-SMA) and collagen at the mRNA and protein levels compared to transforming growth factor beta 1 (TGF-β1)-treated LX-2 cells, leading to the STAT3 pathway inhibition, which finally resulted in hepatoprotective outcomes. Based on the docking results obtained in the present study, pulmatin exhibited four hydrogens as well as four hydrophobic interactions with the Gly183, Leu184, Ala186, Glu223, Ile243, and Tyr244 inside the MMP-13 catalytic site. Two of them are $\pi - \pi$ stack pairing between pulmatin and Gly183 (4.37 Å and 4.95 Å), which are known as the most stabilizing connections [47].

Sennidin A (SA) is a dianthrone extracted from the *Cassia L.*, *Senna*. It was illustrated that it has good solubility and stability against aggregations. As well, in previous studies, the radioiodinated SA (^{131}I-SA) has shown anti-tumor properties [25]. In this regard, Ji et al. [25] reported that the combination of ^{131}I-SA with necrosis-inducing drugs/therapies could considerably lead to tumor growth inhibition in vivo. According to the results of the present study, Sennidin A demonstrated considerable binding affinity to the MMP-13 catalytic domain with $\Delta G_{binding}$ as -9.65 kcal/mol. Moreover, this component revealed three hydrophobic interactions with Leu184, His232, and Pro242 within the active site of the enzyme. The interaction between His232 and Sennidin A was found as a $\pi - \pi$ stack pairing. The estimated $\Delta G_{binding}$ between sennidin B and the MMP-13 active site was predicted to be -8.51 kcal/mol. It was demonstrated that three hydrophobic interactions existed with the Gly183 and Pro242 inside the MMP-13 catalytic site.

Emodin, as a 1,3,8-trihydroxy-6-methylanthraquinone, is commonly found in several Chinese herbs such as *Polygonum cuspidatum* [48], *Rheum palmatum* [49], *Aloe vera* [50], and *Polygonum multiflorum* [51]. Numerous pharmacological actions have been reported in previous studies for emodin, including anticancer, anti-inflammatory, antimicrobial, neuroprotective, and antiosteoporotic properties [52-55]. Ha et al. [31] executed a study to examine the anti-inflammatory effects of emodin on IL-1β and LPS-stimulated rheumatoid arthritis synoviocytes under hypoxia.

As a result, they reported that emodin led to the decreased expression of cyclooxygenase 2 (COX-2), hypoxia-inducible factor 1 alpha (HIF-1α), vascular endothelial growth factor (VEGF),

MMP-1, and MMP-13 at the mRNA level, which resulted in the down-regulation of proinflammatory cytokines, VEGF, and histone deacetylase 1 (HDAC1) in vitro [31]. Liu et al. [32] performed a study to examine the effects of emodin on several inflammatory factors in chondrocytes isolated from rats. The mRNA levels of MMP-3 and MMP-13 were measured using reverse transcription-quantitative polymerase chain reaction (RT-qPCR). In addition, the MMP-3 and MMP-13 expressions were studied at the protein level using western-blot analysis. Finally, they reported that emodin resulted in the down-regulation of MMP-3, MMP-13, and several proteins taking a part in the ERK and Wnt/β-catenin signaling pathways, which led to the enhanced chondrocytes proliferation [32].

According to the results of the present study, it was estimated that emodin can bind to the MMP-13 catalytic site at the nanomolar concentration (*K*i = 279.97 nM) and with a $\Delta G_{binding}$ as -8.94 kcal/mol. As well, Emodin revealed two hydrogen, five hydrophobic, and one lone pair interaction with the Leu185, Ala186, His232, Pro242, and Ile243 within the MMP-13 catalytic site. A π – π stack pairing was observed between emodin and His232 with the bond length estimated as 6.21 Å. The binding affinities of several emodin derivatives to the MMP-13 catalytic domain were also predicted. Emodin-8-glucoside was predicted to be connected to the catalytic domain of MMP-13 with the $\Delta G_{binding}$ and *K*i value of -9.07 and 224.35 nM, respectively. Additionally, one hydrophobic interaction was found with the Leu184. Furthermore, aloe emodin 8-glucoside was observed to be connected to the MMP-13 with the $\Delta G_{binding}$ and *K*i value of -8.49 and 594.84 nM, respectively. One hydrophobic interaction with the Ser182 was demonstrated. Besides, aloe-emodin attached to the MMP-13 active site with the $\Delta G_{binding}$ and *K*i value as -8.23 and 929.88 nM, respectively. Aloe-emodin formed one hydrogen, three hydrophobic, and one lone pair interaction with Leu185, His232, Pro242, and Ile243. A π – π stack pairing was also found between aloe-emodin and His232 (6.20 Å). Aloe-emodin has shown anti-inflammatory effects on arthritis [56-59].

Obtusifolin is an AQ predominantly found in *Senna. obtusifolia* [60], which is widely used for therapeutic aims in several disorders like rheumatism [28]. It has been reported that obtusifolin has some suppressive effects on cancer metastasis and can diminish memory loss and attenuate mitochondrial apoptosis [60-63]. Recently, Nam et al. [27] in their study investigated the effect of obtusifolin on osteoarthritis inflammation in vitro. Thereafter, the authors measured the expressions of MMP-3, MMP-13, COX-2, and prostaglandin E2 (PGE2), as well as several signaling proteins at the mRNA and protein levels using real-time polymerase chain reaction (RT-PCR) and western-blotting techniques, respectively. According to their results, obtusifolin was found to have the abilities of inhibiting the MMP-3, MMP-13, and Cox2 expressions, and decreasing the PGE2 activity, leading to the diminished cartilage injury. According to the results of the present study, obtusifolin can potentially bind to the MMP-13 catalytic domain with a $\Delta G_{binding}$ and a *K*i of -8.10 kcal/mol and 1.15 μM, respectively, illustrating a moderate binding affinity between these two molecules.

Rhodoptilometrin is an AQ isolated from *Himerometra magnipinna* [64,65] that can cause some cytotoxic effects on several cancer cell lines, including MCF-7 breast cancer, SF-268 glioblastoma, and the H460 non-small-cell lung cancer [66]. Tseng et al. [67] demonstrated that rhodoptilometrin could considerably progress the wound healing process, cell migration, and proliferation of human gingival fibroblasts. Moreover, rhodoptilometrin resulted in the overexpression of focal adhesion kinase (FAK), fibronectin, type I collagen, and proteins involved in the mitochondrial complexes I~V, consequently leading to the enhanced gingival regeneration. It is worth mentioning that gingival recession is an oral disorder in which the gum tissue impairment may possibly result in the exposure of the teeth roots that could subsequently cause tooth decay [68], hypersensitivity of dentin [69], and aesthetic problems [70]. Based on our findings, it is estimated that rhodoptilometrin can be connected to the MMP-13 active site at the concentration of 285.97 nM with the $\Delta G_{binding}$ of -8.93 kcal/mol. Therefore, it may be suggested that rhodoptilometrin could be considered as a potential anti-tooth caries compound with two mechanisms: firstly, by promoting the human gingival regeneration, and secondly, via inhibiting the MMP-13 activity.

Rhodoptilometrin demonstrated two hydrogen and five hydrophobic interactions with Leu185, Ala186, Val219, His222, Pro242, and Ile243 inside the MMP-13 catalytic domain.

Chrysophanol is an AQ derivative (1,8-dihydroxy-3-methyl-anthraquinone) extracted from *Rheum undulatum* L. which can be commonly found in China and European countries [71,72]. Various pharmaceutical properties of chrysophanol such as antioxidant, anti-inflammatory, antimicrobial, anti-ageing, and neuroprotective effects have been demonstrated previously [29,30]. Several previous studies have shown anti-tumorigenesis activities of chrysophanol against lung [73,74], colorectal [75,76], oral cancer cell lines [77,78], breast [79,80], prostate [81], ovarian [81], liver [82,83], and cervical cancer [84]. According to our results, it was indicated that chrysophanol can inhibit the MMP-13 activity at the concentration of 338.39 nM with a $\Delta G_{binding}$ of -8.83 kcal/mol. One hydrogen, five hydrophobic, and one loan pair interactions with the amino acids were found inside the active site of the MPP-13.

To study the stability of the docked pose between the top-10 AQs and MMP-13 active site, the interactions between the compounds and the residues of the protein were compared in terms of before and after the molecular dynamics simulations. Accordingly, it was observed that the docked poses of pulmatin, emodin-8-glucoside, emodin, rhodoptilometrin, chrysophanol, knipholone, aloeeEmodin 8-glucoside, and aloe-emodin within the MMP-13 active site were considerably stable; therefore, these AQs can be considered as the effective inhibitors of MMP-13. In this regard, the following points can be mentioned:

1. Pulmatin demonstrated two hydrogen bonds, including one classical and one non-classical H-bonds, after the molecular dynamics simulation. The interaction between pulmatin and Glu223 was found to be stable after the molecular dynamics simulation, as well.
2. Emodin-8-glucoside revealed four hydrogen bonds, including one classical and three non-classical H-bonds, after the molecular dynamics simulation.
3. Emodin showed two classical H-bonds after the molecular dynamics simulations.
4. Rhodoptilometrin illustrated one classical H-bond and six hydrophobic interactions, including three stabilizing π–π interactions, after the molecular dynamics simulation. The interaction between rhodoptilometrin and Val219 was found to be stable after the molecular dynamics simulation.
5. Chrysophanol exhibited three hydrogens (including two classical and one non-classical H-bond) as well as four hydrophobic interactions (three of which were π–π stabilizing interactions) after the MD simulation.
6. Knipholone had three classical H-bonds as well as nine hydrophobic interactions (two of which were π–π stabilizing interactions) after the MD simulation. Of note, the interaction between knipholone and Pro242 was found to be stable after the MD simulation.
7. Aloe emodin 8-glucoside formed five hydrogen interactions after the MD simulation, one of which was classical H-bond.
8. Aloe emodin revealed four hydrogen interactions (including three classical and one non-classical H-bond) as well as five hydrophobic interactions (including two π–π stabilizing interactions and three pi-alkyl interactions) after the MD simulation.

Moreover, sennidin B only performed one hydrogen bond after the MD simulation; therefore, it may be suggested that the docked pose of sennidin B was not considerably stable inside the MMP-13 catalytic domain. In addition, sennidin A revealed no interaction with the residues of the MMP-13 after the MD simulation, so it could not be considered as a stable inhibitor of the MMP-13. Figure 3 shows the three-dimensional docked poses of the top-10 AQs within the MMP-13 active site before and after the MD simulations.

Conclusion

In the present study, a total of 21 AQs were docked to the MMP-13 active site using the AutoDock 4.0 software, to estimate the binding affinity of these plant-based compounds to the target protein. The stability of the docked poses of the top ranked AQs was examined in a 1ns simulation. The results showed that pulmatin, sennidin A, emodin-8-glucoside, emodin, rhodoptilometrin, chrysophanol, knipholone, sennidin B, aloe emodin 8-glucoside, and aloe-emodin possessed considerable binding affinities to the active site residues of the MMP-13. However, by conducting the MD simulations, it

was revealed that the docked poses of sennidin A and sennidin B were not considerably stable. The chemo-physical analysis showed that, except sennidin A and sennidin B, all top-ranked AQs could be considered as orally active drugs. Nevertheless, the efficacy of these compounds must be examined using experimental approaches in future studies, to reach more effective compounds for therapeutic applications in several human disorders, including cancer, Alzheimer's disease, osteoarthritis, skin ageing, and dental caries.

Acknowledgments

We would like to thank the Deputy of Research and Technology, Dental Research Center and Research Center for Molecular Medicine, Hamadan University of Medical Sciences, Hamadan, Iran, for their supports.

Author contributions

Amir Taherkhani and Zahra Khamverdi designed the study. Molecular Docking and bioavailability analyses were performed by Amir Taherkhani. All Figures were prepared by Amir Taherkhani. The results were analyzed and discussed by Amir Taherkhani, Zahra Khamverdi, Shirin Moradkhani, Athena Orangi, and Alireza Jalalvand. Amir Taherkhani wrote the manuscript. All authors read and approved the final version of the manuscript.

Declaration of interest

The authors declare that there is no conflict of interest. The authors alone are responsible for the accuracy and integrity of the paper content.

References

[1] Jacobsen JA, Jourden JLM, Miller MT, Cohen SM. To bind zinc or not to bind zinc: an examination of innovative approaches to improved metalloproteinase inhibition. *Biochim Biophys Acta Mol Cell Res*. 2010; 1803(1): 72–94.

[2] Taherkhani A, Moradkhani S, Orangi A, Jalalvand A, Khamverdi Z. Molecular docking study of flavonoid compounds for possible matrix metalloproteinase-13 inhibition. *J Basic Clin Physiol Pharmacol*. 2020; Article ID 20200036.

[3] Wan Y, Li W, Liao Z, Yan M, Chen X, Tang Z. Selective MMP-13 inhibitors: promising agents for the therapy of osteoarthritis. *Curr Med Chem*. 2020; 27(22): 3753–3769.

[4] Li NG, Shi ZH, Tang YP, Wang ZJ, Song SL, Qian LH, Qian DW, Duan JA. New hope for the treatment of osteoarthritis through selective inhibition of MMP-13. *Curr Med Chem*. 2011; 18(7): 977–1001.

[5] Moore BA, Aznavoorian S, Engler JA, Windsor LJ. Induction of collagenase-3 (MMP-13) in rheumatoid arthritis synovial fibroblasts. *Biochim Biophys Acta*. 2000; 1502(2): 307–318.

[6] Leeman MF, Curran S, Murray GI. The structure, regulation, and function of human matrix metalloproteinase-13. *Crit Rev Biochem Mol Biol*. 2002; 37(3): 149–166.

[7] Li JJ, Johnson AR. Selective MMP13 inhibitors. *Med Res Rev*. 2011; 31(6): 863–894.

[8] Chaussain-Miller C, Fioretti F, Goldberg M, Menashi S. The role of matrix metalloproteinases (MMPs) in human caries. *J Dent Res*. 2006; 85(1): 22–32.

[9] Hannas AR, Pereira JC, Granjeiro JM, Tjäderhane L. The role of matrix metalloproteinases in the oral environment. *Acta Odontol Scand*. 2007; 65(1): 1–13.

[10] Shimada Y, Ichinose S, Sadr A, Burrow M, Tagami J. Localization of matrix metalloproteinases (MMPs-2, 8, 9 and 20) in normal and carious dentine. *Aust Dent J*. 2009; 54(4): 347–354.

[11] Maciejczyk M, Pietrzykowska A, Zalewska A, Knaś M, Daniszewska I. The significance of matrix metalloproteinases in oral diseases. *Adv Clin Exp Med*. 2016; 25(2): 383–390.

[12] Vasconcelos KR, Arid J, Evangelista S, Oliveira S, Dutra AL, Silva LAB, Segato RAB, Viera AR, Nelson-Filho P, Küchler EC. MMP13 contributes to dental caries associated with developmental defects of enamel. *Caries Res*. 2019; 53(4): 441–446.

[13] Uzun M, Guvenalp Z, Kazaz C, Demirezer LO. Matrix metalloproteinase inhibitor and sunscreen effective compounds from *Rumex crispus* L.: isolation, identification, bioactivity and molecular docking study. *Phytochem Anal*. 2020; 31(6): 818–834.

[14] Chu H, He QX, Wang JW, Deng YT, Wang J, Hu Y, Wang YQ, Lin Z. 3D-QSAR, molecular docking, and molecular dynamics simulation of a novel thieno[3,4-d] pyrimidine inhibitor targeting human immunodeficiency virus type 1 reverse

transcriptase. *J Biomol Struct Dyn*. 2020; 38(15): 4567–4578.

[15] Kumar Y, Singh H, Patel CN. In silico prediction of potential inhibitors for the main protease of SARS-CoV-2 using molecular docking and dynamics simulation based drug-repurposing. *J Infect Public Health*. 2020; 13(9): 1210–1223.

[16] Taherkhani A, Orangi A, Moradkhani S, Khamverdi Z. Molecular docking analysis of flavonoid compounds with matrix metalloproteinase-8 for the identification of potential effective inhibitors. *Lett Drug Des Discov*. 2021; 18(1): 16–45.

[17] Xu Z, Peng C, Shi Y, Zhu Z, Mu K, Wang X, Zhu W. Nelfinavir was predicted to be a potential inhibitor of 2019-nCov main protease by an integrative approach combining homology modelling, molecular docking and binding free energy calculation. *Bio Rxiv*. 2020; Article ID 921627.

[18] Hosseini M, Chen W, Xiao D. Computational molecular docking and virtual screening revealed promising SARS-CoV-2 drugs. *Precis Clin Med.* 2021; 4(1): 1–16.

[19] Chen W, Li A, Wang J, Zhong H, Yuan J, Luo Y, Ou J, Chen J, Li L. A combined approach of QSAR study, molecular docking and pharmacokinetics prediction of promising Amide-Ac6-aminoacetonitriles Cathepsin K inhibitors. *J Mol Struct*. 2021; Article ID 130772.

[20] Choi J, Yun JS, Song H, Shin YK, Kang YH, Munashingha PR, Yoon J, Kim NH, Kim HS, Yook J. Prediction of african swine fever virus inhibitors by molecular docking-driven machine learning models. *Molecules*. 2021; 26(12): 1–12.

[21] Das S, Sarmah S, Lyndem S, Singha Roy A. An investigation into the identification of potential inhibitors of SARS-CoV-2 main protease using molecular docking study. *J Biomol Struct Dyn*. 2021; 39(9): 3347–3357.

[22] Benalla W, Bellahcen S, Bnouham M. Antidiabetic medicinal plants as a source of alpha glucosidase inhibitors. *Curr Diabetes Rev*. 2010; 6(4): 247–254.

[23] Tikhomirov AS, Shtil AA, Shchekotikhin AE. Advances in the discovery of anthraquinone-based anticancer agents. *Recent Pat Anticancer Drug Discov*. 2018; 13(2): 159–183.

[24] Diaz-Munoz G, Miranda IL, Sartori SK, De Rezende DC, Diaz MA. Anthraquinones: an overview. *Stud Nat Prod Chem*. 2018; 58: 313–338.

[25] Ji Y, Jiang C, Zhang X, Liu W, Gao M, Li Y, Wang J, Wang Q, Sun Z, Jiang Z. Necrosis targeted combinational theragnostic approach to treat cancer. *Oncotarget*. 2014; 5(10): 2934–2946.

[26] Siddamurthi S, Gutti G, Jana S, Kumar A, Singh SK. Anthraquinone: a promising scaffold for the discovery and development of therapeutic agents in cancer therapy. *Future Med Chem*. 2020; 12(11): 1037–1069.

[27] Nam J, Seol DW, Lee CG, Wee G, Yang S, Pan CH. Obtusifolin, an anthraquinone extracted from *Senna obtusifolia* (L.) H.S. Irwin & Barneby, reduces inflammation in a mouse osteoarthritis model. *Pharmaceuticals.* 2021; 14(3): 1–9.

[28] Kowalczyk T, Sitarek P, Toma M, Picot L, Wielanek M, Skała E, Sliwinski T. An extract of transgenic *Senna obtusifolia* L. hairy roots with overexpression of PgSS1 gene in combination with chemotherapeutic agent induces apoptosis in the leukemia cell line. *Biomolecules*. 2020; 10(4): 1–20.

[29] Xie L, Tang H, Song J, Long J, Zhang L, Li X. Chrysophanol: a review of its pharmacology, toxicity and pharmacokinetics. *J Pharm Pharmacol*. 2019; 71(10): 1475–1487.

[30] Yusuf MA, Singh BN, Sudheer S, Kharwar RN, Siddiqui S, Abdel-Azeem AM, Fernandes Fraceto L, Dashora K, Gupta VK. Chrysophanol: a natural anthraquinone with multifaceted biotherapeutic potential. *Biomolecules*. 2019; 9(2): 1–24.

[31] Ha MK, Song YH, Jeong SJ, Lee HJ, Jung JH, Kim B, Song HS, Huh JE, Kim SH. Emodin inhibits proinflammatory responses and inactivates histone deacetylase 1 in hypoxic rheumatoid synoviocytes. *Biol Pharm Bull*. 2011; 34(9): 1432–1437.

[32] Liu Z, Lang Y, Li L, Liang Z, Deng Y, Fang R, Meng Q. Effect of emodin on chondrocyte viability in an in vitro model of osteoarthritis. *Exp Ther Med*. 2018; 16(6): 5384–5389.

[33] Deshpande N, Addess KJ, Bluhm WF, Merino-Ott JC, Townsend-Merino W, Zhang Q, Knezevich C, Xie L, Chen L, Feng Z. The RCSB protein data bank: a redesigned query system and relational database based on the mmCIF schema. *Nucleic Acids Res*. 2005; 33:

233–237.
[34] Kim S, Thiessen PA, Bolton EE, Chen J, Fu G, Gindulyte A, Han L, He J, He S, Shoemaker BA. PubChem substance and compound databases. *Nucleic Acids Res*. 2016; 44(D1): 1202–1213.
[35] Nara H, Kaieda A, Sato K, Naito T, Mototani H, Oki H, Yamamoto Y, Kuno H, Santou T, Kanzaki N. Discovery of novel, highly potent, and selective matrix metalloproteinase (MMP)-13 inhibitors with a 1, 2, 4-triazol-3-yl moiety as a zinc binding group using a structure-based design approach. *J Med Chem*. 2017; 60(2): 608–626.
[36] Guex N, Peitsch MC, Schwede T. Automated comparative protein structure modeling withnam SWISS-MODEL and Swiss-PdbViewer: a historical perspective. *Electrophoresis*. 2009; 30(S): 162–173.
[37] Laxmi D, Priyadarshy S. HyperChem 6.03. *Biotech Software Internet Rep*. 2002; 3(1): 5–9.
[38] Morris GM, Huey R, Lindstrom W, Sanner MF, Belew RK, Goodsell DS, Olson A. AutoDock4 and AutoDockTools4: automated docking with selective receptor flexibility. *J Comput Chem*. 2009; 30(16): 2785–2791.
[39] Lipinski CA, Lombardo F, Dominy BW, Feeney PJ. Experimental and computational approaches to estimate solubility and permeability in drug discovery and development settings. *Adv Drug Deliv Rev*. 1997; 23(1-3): 3–25.
[40] Saito R, Smoot ME, Ono K, Ruscheinski J, Wang PL, Lotia S, Pico A, Bader GD, Ideker T. A travel guide to cytoscape plugins. *Nat Methods*. 2012; 9(11): 1069–1076.
[41] Zhu BL, Long Y, Luo W, Yan Z, Lai YJ, Zhao LG, Zhou WH, Wang YJ, Shen LL, Liu L. MMP13 inhibition rescues cognitive decline in Alzheimer transgenic mice via BACE1 regulation. *Brain*. 2019; 142(1): 176–192.
[42] Balbín M, Pendás AM, Uría JA, Jiménez MG, Freije JP, López-Otín C. Expression and regulation of collagenase-3 (MMP-13) in human malignant tumors. *Apmis*. 1999; 107(1): 45–53.
[43] Kamil M, Haque E, Mir SS, Irfan S, Hasan A, Sheikh S, Alam S, Ansari KM, Nazir M. Hydroxyl group difference between anthraquinone derivatives regulate different cell death pathways via nucleo-cytoplasmic shuttling of p53. *Anticancer Agents Med Chem*. 2019; 19(2): 184–193.
[44] Seo EJ, Ngoc TM, Lee SM, Kim YS, Jung YS. Chrysophanol-8-O-glucoside, an anthraquinone derivative in rhubarb, has antiplatelet and anticoagulant activities. *J Pharmacol Sci*. 2012; 118(2): 245–254.
[45] Park YJ, Lee KH, Jeon MS, Lee YH, Ko YJ, Pang C, Kim B, Chung KH, Kim KH. Hepatoprotective potency of chrysophanol 8-O-glucoside from *Rheum palmatum* L. against hepatic fibrosis via regulation of the STAT3 signaling pathway. *Int J Mol Sci*. 2020; 21(23): 1–12.
[46] Siegers C, Von Hertzberg-Lottin E, Otte M, Schneider B. Anthranoid laxative abuse-a risk for colorectal cancer? *Gut*. 1993; 34(8): 1099–1101.
[47] Muthusamy K, Prasad S, Nagamani S. Role of hydrophobic patch in LRP6: a promising drug target for Alzheimer's disease. *Indian J Pharm Sci*. 2016; 78(2): 240–251.
[48] Wang W, Zhou Q, Liu L, Zou K. Anti-allergic activity of emodin on IgE-mediated activation in RBL-2H3 cells. *Pharmacol Rep*. 2012; 64(5): 1216–1222.
[49] Wang JB, Zhao HP, Zhao YL, Jin C, Liu DJ, Kong WJ, Fang F, Zhang L, Wang HJ, Xiao XH. Hepatotoxicity or hepatoprotection? pattern recognition for the paradoxical effect of the Chinese herb *Rheum palmatum* L. in treating rat liver injury. *PLoS One*. 2011; 6(9): 1–8.
[50] Naqvi S, Ullah M, Hadi S. DNA degradation by aqueous extract of *Aloe vera* in the presence of copper ions. *Indian J Biochem Biophys.* 2010; 47(3): 161–165.
[51] Lee MH, Kao L, Lin CC. Comparison of the antioxidant and transmembrane permeative activities of the different *Polygonum cuspidatum* extracts in phospholipid-based microemulsions. *J Agric Food Chem*. 2011; 59(17): 9135–9141.
[52] Shrimali D, Shanmugam MK, Kumar AP, Zhang J, Tan BK, Ahn KS, Sethi G. Targeted abrogation of diverse signal transduction cascades by emodin for the treatment of inflammatory disorders and cancer. *Cancer Lett*. 2013; 341(2): 139–149.
[53] Wei WT, Lin SZ, Liu DL, Wang ZH. The distinct mechanisms of the antitumor activity of emodin in different types of cancer. *Oncol*

Rep. 2013; 30(6): 2555–2562.
[54] Dong X, Fu J, Yin X, Cao S, Li X, Lin L, Huyiligeqi, Ni J. Emodin: a review of its pharmacology, toxicity and pharmacokinetics. *Phytother Res*. 2016; 30(8): 1207–1218.
[55] Matsuda Y, Yokohira M, Suzuki S, Hosokawa K, Yamakawa K, Zeng Y, Ninomiya F, Saoo K, Kuno T, Imaida K. One-year chronic toxicity study of *Aloe arborescens* Miller var. *natalensis* Berger in Wistar Hannover rats. A pilot study. *Food Chem Toxicol*. 2008; 46(2): 733–739.
[56] Hou J, Gu Y, Zhao S, Huo M, Wang S, Zhang Y, Qiao Y, Li X. Anti-inflammatory effects of aurantio-obtusin from seed of *Cassia obtusifolia* L. through modulation of the NF-κB pathway. *Molecules*. 2018; 23(12): 1–15.
[57] Wang H, Yang D, Li L, Yang S, Du G, Lu Y. Anti-inflammatory effects and mechanisms of rhein, an anthraquinone compound, and its applications in treating arthritis: a review. *Nat Prod Bioprospecting*. 2020: 10(6): 445–452.
[58] Ding QH, Ye CY, Chen EM, Zhang W, Wang XH. Emodin ameliorates cartilage degradation in osteoarthritis by inhibiting NF-κB and Wnt/β-catenin signaling in-vitro and in-vivo. *Int Immunopharmacol*. 2018; 61: 222–230.
[59] Kshirsagar AD, Panchal PV, Harle UN, Nanda RK, Shaikh HM. Anti-inflammatory and antiarthritic activity of anthraquinone derivatives in rodents. *Int J Inflamm*. 2014; Article ID 690596.
[60] Xu L, Chan Co, Lau CC, Yu Z, Mok DK, Chen S. Simultaneous determination of eight anthraquinones in semen Cassiae by HPLC-DAD. *Phytochem Anal*. 2012; 23(2): 110–116.
[61] Tang Y, Zhong ZY, Liu YF, Sheng GT. Obtusifolin inhibits high glucose-induced mitochondrial apoptosis in human umbilical vein endothelial cells. *Mol Med Rep*. 2018; 18(3): 3011–3019.
[62] Kim DH, Hyun SK, Yoon BH, Seo JH, Lee KT, Cheong JH, Jung SY, Jin C, Choi JS, Ryu JH. Gluco-obtusifolin and its aglycon, obtusifolin, attenuate scopolamine-induced memory impairment. *J Pharmacol Sci*. 2009; 111(2): 110–116.
[63] Hsu YL, Tsai EM, Hou MF, Wang TN, Hung JY, Kuo PL. Obtusifolin suppresses phthalate esters-induced breast cancer bone metastasis by targeting parathyroid hormone-related protein. *J Agric Food Chem*. 2014; 62(49): 11933–11940.
[64] Lin YY, Tsai SJ, Chiang MY, Wen ZH, Su JH. Anti-inflammatory anthraquinones from the crinoid *Himerometra magnipinna*. *Nat Prod Commun*. 2015; 10(2): 317–318.
[65] Shao N, Yao G, Chang LC. Bioactive constituents from the marine crinoid *Himerometra magnipinna. J Nat Prod*. 2007; 70(5): 869–871.
[66] Wright AD, Nielson JL, Tapiolas DM, Motti CA, Ovenden SP, Kearns PS, Liptrot CH. Detailed NMR, including 1, 1-ADEQUATE, and anticancer studies of compounds from the echinoderm *Colobometra perspinosa. Mar Drugs*. 2009; 7(4): 565–575.
[67] Tseng CC, Lai YC, Kuo TJ, Su JH, Sung PJ, Feng CW, Lin YY, Chen PC, Tai MH, Cheng SY. Rhodoptilometrin, a crinoid-derived anthraquinone, induces cell regeneration by promoting wound healing and oxidative phosphorylation in human gingival fibroblast cells. *Mar Drugs*. 2019; 17(3): 1–20.
[68] Hellyer P, Beighton D, Heath M, Lynch E. Root caries in older people attending a general dental practice in East Sussex. *Br Dent J*. 1990; 169(7): 201–206.
[69] Al-Wahadni A, Linden GJ. Dentine hypersensitivity in Jordanian dental attenders: a case control study. *J Clin Periodontol*. 2002; 29(8): 688–693.
[70] Kassab MM, Cohen RE. The etiology and prevalence of gingival recession. *J Am Dent Assoc*. 2003; 134(2): 220–225.
[71] Malik S, Sharma N, Sharma UK, Singh NP, Bhushan S, Sharma M, Sinha AH, Ahuja PS. Qualitative and quantitative analysis of anthraquinone derivatives in rhizomes of tissue culture-raised *Rheum emodi* Wall. plants. *J Plant Physiol*. 2010; 167(9): 749–756.
[72] Sun SW, Yeh PC. Analysis of rhubarb anthraquinones and bianthrones by microemulsion electrokinetic chromatography. *J Pharm Biomed Anal*. 2005; 36(5): 995–1001.
[73] Zhang J, Wang Q, Wang Q, Guo P, Wang Y, Xing Y, Zhang M, Liu F, Qingyun Z. Retraction note to: chrysophanol exhibits anti-cancer activities in lung cancer cell through regulating ROS/HIF-1a/VEGF

signaling pathway. *Naunyn Schmiedebergs Arch Pharmacol.* 2021; 394(3): 577–578.
[74] Ni CH, Yu CS, Lu HF, Yang JS, Huang HY, Chen PY, Wu SH, Ip SW, Chiang SY, Lin JG. Chrysophanol-induced cell death (necrosis) in human lung cancer A549 cells is mediated through increasing reactive oxygen species and decreasing the level of mitochondrial membrane potential. *Environ Toxicol*. 2014; 29(7): 740–749.
[75] Deng M, Xue Y, Xu L, Wang Q, Wei J, Ke X, Wang J, Chen X. Chrysophanol exhibits inhibitory activities against colorectal cancer by targeting decorin. *Cell Biochem Funct.* 2020; 38(1): 47–57.
[76] Shen L, Yang W. Molecular dynamics simulations with quantum mechanics/molecular mechanics and adaptive neural networks. *J Chem Theory Comput*. 2018; 14(3): 1442–1455.
[77] Hsu PC, Cheng CF, Hsieh PC. Chrysophanol regulates cell death, metastasis, and reactive oxygen species production in oral cancer cell lines. *Evid Based Complement Alternat Med*. 2020; Article ID 5867064.
[78] Chung PC, Hsieh PC, Lan CC, Hsu PC, Sung MY, Lin YH, Tzeng IS, Chiu V, Cheng CF, Kuo CY. Role of chrysophanol in epithelial-mesenchymal transition in oral cancer cell lines via a Wnt-3-dependent pathway. *Evid Based Complement Altern Med.* 2020; Article ID 8373715.
[79] Ren L, Li Z, Dai C, Zhao D, Wang Y, Ma C, Liu C. Chrysophanol inhibits proliferation and induces apoptosis through NF-κB/cyclin D1 and NF-κB/Bcl-2 signaling cascade in breast cancer cell lines. *Mol Med Rep*. 2018; 17(3): 4376–4382.
[80] Park S, Lim W, Song G. Chrysophanol selectively represses breast cancer cell growth by inducing reactive oxygen species production and endoplasmic reticulum stress via AKT and mitogen-activated protein kinase signal pathways. *Toxicol Appl Pharmacol*. 2018; 360: 201–211.
[81] Lu L, Li K, Mao YH, Qu H, Yao B, Zhong WW, Ma B, Wang ZY. Gold-chrysophanol nanoparticles suppress human prostate cancer progression through inactivating AKT expression and inducing apoptosis and ROS generation in vitro and in vivo. *Int J Oncol*. 2017; 51(4): 1089–1103.
[82] Lu CC, Yang JS, Huang AC, Hsia TC, Chou ST, Kuo CL, Lu HF, Lee TH, Wood WG, Chung JG. Chrysophanol induces necrosis through the production of ROS and alteration of ATP levels in J5 human liver cancer cells. *Mol Nutr Food Res*. 2010; 54(7): 967–976.
[83] Ni CH, Chen PY, Lu HF, Yang JS, Huang HY, Wu SH, Ip SW, Wu CT, Chiang SY, Lin JG, Wood WG, Chung JG. Chrysophanol-induced necrotic-like cell death through an impaired mitochondrial ATP synthesis in Hep3B human liver cancer cells. *Arch Pharm Res*. 2012; 35(5): 887–895.
[84] Trybus W, Król T. The potential antitumor effect of chrysophanol in relation to cervical cancer cells. *J Cell Biochem*. 2021; 122(6): 639–652.

Abbreviations

MMPs: matrix metalloproteinases; AQs: anthraquinones; MD: molecular dynamics; RCSB: Research Collaboratory for Structural Bioinformatics; LogP: log of the partition coefficient between octanol and water; *K*i: inhibition constant; α-SMA: smooth muscle alpha-actin; TGF-β1: transforming growth factor beta 1; COX-2: cyclooxygenase 2; HIF-1α: hypoxia-inducible factor 1 alpha; VEGF: vascular endothelial growth factor; HDAC1: histone deacetylase 1; RT-qPCR: reverse transcription-quantitative polymerase chain reaction; PGE2: prostaglandin E2; RT-PCR: real-time polymerase chain reaction; FAK: focal adhesion kinase.